Gemini/GRACES spectroscopy of stars in Tri II

K. Venn, E. Starkenburg, L. Malo, N. Martin, B. Laevens

Monthly Notices
of the
ROYAL ASTRONOMICAL SOCIETY

MNRAS **466,** 3741–3752 (2017)
Advance Access publication 2016 December 10

doi:10.1093/mnras/stw3198

Gemini/GRACES spectroscopy of stars in Tri II

K. A. Venn,[1]★ E. Starkenburg,[2] L. Malo,[3] N. Martin[4,5] and B. P. M. Laevens[6]

[1]*Department of Physics and Astronomy, University of Victoria, Victoria, BC V8W 3P2, Canada*
[2]*Leibniz-Institut für Astrophysik Potsdam (AIP), An der Sternwarte 16, D-14482 Potsdam, Germany*
[3]*Canada-France-Hawaii Telescope Corporation, 65-1238 Mamalahoa Highway, Kamuela, HI 96743, USA*
[4]*Observatoire astronomique de Strasbourg, Université de Strasbourg, CNRS, F-67000 Strasbourg, France*
[5]*Max-Planck-Institut für Astronomie, Königstuhl 17, D-69117 Heidelberg, Germany*
[6]*Institute of Astrophysics, Pontificia Universidad Católica de Chile, Av. Vicuña Mackenna 4860, 7820436 Macul, Santiago, Chile*

Accepted 2016 December 6. Received 2016 December 5; in original form 2016 July 31

ABSTRACT

The chemical abundance ratios and radial velocities for two stars in the recently discovered Triangulum II faint dwarf galaxy have been determined from high-resolution, medium signal-to-noise ratio spectra from the Gemini Remote Access to CFHT ESPaDonS Spectrograph facility. These stars have stellar parameters and metallicities similar to those derived from their photometry and medium-resolution Ca II triplet spectra, and supports that Triangulum II has a metallicity spread consistent with chemical evolution in a dwarf galaxy. The elemental abundances show that both stars have typical calcium abundances and barium upper limits for their metallicities, but low magnesium and sodium. This chemical composition resembles some stars in dwarf galaxies, attributed to inhomogeneous mixing in a low star formation environment, and/or yields from only a few supernova events. One of our targets (Star40) has an enhancement in potassium, and resembles some stars in the unusual outer halo star cluster, NGC 2419. Our other target (Star46) appears to be a binary based on a change in its radial velocity ($\Delta v_{\rm rad} = 24.5 \pm 2.1\,{\rm km\,s^{-1}}$). This is consistent with variations found in binary stars in other dwarf galaxies. While this serves as a reminder of the high binary fraction in these ultrafaint dwarf galaxies, this particular object has had little impact on the previous determination of the velocity dispersion in Triangulum II.

Key words: stars: abundances – galaxies: dwarf – galaxies: individual: Triangulum II.

1 INTRODUCTION

In the preferred cold dark matter cosmological paradigm, numerous faint galaxies are predicted to surround the Galaxy (Tollerud et al. 2008; Bullock et al. 2010; Hargis et al. 2014). Deep imaging surveys have recently discovered several faint satellites (e.g. Bechtol et al. 2015; Kim & Jerjen 2015; Laevens et al. 2015 a), yet confirming their nature as dwarf galaxies requires spectroscopic follow-up, e.g. to distinguish these objects from diffuse globular clusters, which would be dynamically cold and show no significant metallicity dispersions indicative of self-enrichment (Tolstoy, Hill & Tosi 2009; McConnachie 2012; Belokurov 2013). The list of spectroscopically confirmed ultrafaint dwarf galaxies with $M_{\rm V} > -4$ now includes Willman 1 (Willman et al. 2005, 2011), Segue 1 (Geha et al. 2009; Frebel, Simon & Kirby 2014), Draco II (Martin et al. 2016a), Horologium I (Koposov et al. 2015) and Reticulum II (Ret II; Kirby et al. 2015; Koposov et al. 2015; Simon et al. 2015b). Segue 2 also appears to be an ultrafaint dwarf galaxy, but one that retained SNe Ia material and had an extended star formation history despite its presently small mass, leading Kirby et al. (2013) to suggest it is an ultrafaint dwarf galaxy that has experienced tidal stripping. Bootes II is an unusual dwarf galaxy, which shows complicated dynamics that are not expected to reflect its original dynamical mass (Koch et al. 2009).

The recent discovery of Triangulum II (Tri II) in the Pan-STARRS 1 survey (Laevens et al. 2015) provides a new candidate ultrafaint dwarf galaxy ($M_{\rm V} = -1.8 \pm 0.5$) that is only 30 ± 2 kpc from the Sun (or 36 ± 2 kpc from the Galactic Centre). Two independent studies of the Calcium II triplet (CaT) features near λ8500 using Keck/DEep Imaging Multi-Object Spectrograph (DEIMOS, Faber et al. 2003) medium-resolution spectroscopy have provided a velocity dispersion measurement of 4–5 km s^{-1}(Kirby et al. 2015; Martin et al. 2016b) in the central 2′ region, corresponding to a mass-to-light ratio of ∼3600 $M_\odot\ L_\odot^{-1}$. However, Martin et al. (2016b) further suggest that Tri II has complex internal dynamics based on an apparent rise in the velocity dispersion ($14 \pm 5\,{\rm km\,s^{-1}}$) in the outer regions, that could also raise the mean velocity dispersion in this system to $\sim 10\,{\rm km\,s^{-1}}$ with a corresponding half-light radius mass-to-light ratio of 15 500 $M_\odot\ L_\odot^{-1}$. If Tri II is in dynamical

★ E-mail: kvenn@uvic.ca

equilibrium (a challenging assumption given it is <40 kpc from the Galactic Centre and its complex internal dynamics), and its velocity dispersion is confirmed at the higher value, then Tri II would have the highest density of dark matter of any known system. It would be an ideal candidate for indirect detection of dark matter through annihilation interactions (Drlica-Wagner et al. 2015; Geringer-Sameth, Koushiappas & Walker 2015; Hayashi et al. 2016).

The CaT observations of the brightest two red giant branch (RGB) stars in Tri II suggest a mean metallicity $\langle$[Fe/H]$\rangle = -2.6 \pm 0.2$ (Kirby et al. 2015; Martin et al. 2016b), lower than most metal-poor globular clusters; the full sample of RGB stars further suggests a metallicity spread of Δ[Fe/H] = 0.8. More detailed information is available from high-resolution spectroscopy ($R > 10\,000$); detailed spectroscopy of even just a few of the brightest stars in dwarf galaxies can provide insights into differences in the processes of chemical evolution that have occurred there, when compared with stars in the Galactic halo, globular clusters and dwarf galaxies (Venn et al. 2004; Tolstoy et al. 2009; Frebel & Norris 2015). For example, many stars in dwarf spheroidal (dSph) galaxies tend to be *alpha challenged*, where [α/Fe] ~0 at lower metallicities ([Fe/H] ≤ -0.5) than is seen in the Galaxy. On the other hand, some dSph galaxies can also show peculiar abundance patterns. For example, Koch et al. (2008b) showed that two stars in the faint dwarf galaxy Hercules have strongly enhanced alpha-element abundances (e.g. [Mg/Fe] = +0.8) and no detectable heavy element spectral lines, indicating the lowest [Ba/Fe] (<−2 dex) abundances known at that time. Koch et al. suggested that these abundance ratios are consistent with chemical enrichment from a single (or very few) high-mass SNe II (~35 $M_{\odot}$). Similarly, Frebel et al. (2014) found that stars in Segue 1 are also alpha-rich ([α/Fe] ~ 0.5) and lack of neutron capture elements, e.g. [Ba/H] < −4.2, over a wide range of metallicity (−3.8 < [Fe/H] < −1.4), suggesting a lack of iron enrichment from SNe Ia. As in Hercules, these Segue 1 abundances are interpreted as enrichment exclusively from high-mass SNe II, and with no evidence for substantial chemical evolution, thus Segue 1 is regarded as a surviving first galaxy. On the other hand, one of the new ultrafaint dwarf galaxies discovered through the Dark Energy Survey (Bechtol et al. 2015), Ret II, has been found to have amongst the highest [Ba/Fe] abundances at low metallicities; this is a very exciting discovery in terms of identifying potential sources for the rapid-neutron capture site (Ji et al. 2016; Roederer et al. 2016).

In this paper, we present a high-resolution spectral analysis of the two brightest members of Tri II (Star40 and Star46) based on Gemini Remote Access to CFHT ESPaDonS Spectrograph (GRACES) observations. While two stars are a very small sample, we are limited by the brightness of the other known members of Tri II, which are too faint for high-resolution spectroscopic observations with 6–10 m class telescopes. Two stars are still sufficient to examine the nature of Tri II as a ultra faint dwarf galaxy, by studying their chemistry and searching for star-to-star chemical inhomogeneities. These two stars can also contribute to the chemistry of stars in dwarf galaxies when considered as an ensemble.

2 TARGETS, OBSERVATIONS AND DATA REDUCTION

CaT surveys of the brightest stars in the Tri II area have been carried out by Martin et al. (2016b) and Kirby et al. (2015). Both determined similar mean radial velocity (RV) and [Fe/H] values for Tri II, and particularly for the two brightest stars associated with this new ultrafaint dwarf galaxy (see Tables 1 and 2). Optical spectra were taken using the GRACES[1] (Chené et al. 2014; ESPaDonS, Donati 2003) using the two-fibre mode during a Director's Discretionary Time program (GN-2015B-DD-2). Observations were taken during grey time on 2015 December 15–17, and reduced using an adapted version of the OPERA data reduction pipeline (Martioli et al. 2012) for the GRACES data (Malo L. in preparation). Two 30-min exposures were sufficient to reach a signal-to-noise ratio (SNR) = 40 at 6000 Å for Star40 (V = 17.3), whereas four 40-min exposures provided only SNR ~ 10 for Star46 (V = 18.8). This latter SNR was lower than expected, thus we reviewed the acquisition image and do confirm that the correct target was selected. The SNR varied over the useable spectral range (~5000–9000 Å), primarily varying across each echelle order. We calculated the RV solution for each star from a variety of features across each of the unnormalized, wavelength calibrated, sky-subtracted OPERA pipeline spectra. Heliocentric corrections were applied directly by the OPERA pipeline. Spectral co-addition, continuum normalization and line measurements were performed with IRAF.[2] No telluric standards were taken, and we note that the sky subtraction was imperfect,[3] leaving some residual features in our final spectra (e.g. see Figs 3 and 4).

Table 1. Observables.

Observable	Star40	Star46
Name (2MASS)	2M02131654+3610457	–
Name (Kirby et al. 2015)	106	65
RA (J2000)	02 13 16.55	02 13 21.54
Dec. (J2000)	+36 10 45.8	+36 09 57.4
$R_{\rm TriII}$[a]	0.2	1.1
$g_{\rm PI}$	17.585 ± 0.006	19.286 ± 0.013
$r_{\rm PI}$	16.987 ± 0.005	18.778 ± 0.007
$i_{\rm PI}$	16.692 ± 0.004	18.540 ± 0.006
K (2MASS)	14.766	–
V (GSC)[b]	17.25	18.83
V (Kirby et al. 2015)	17.10	18.85
I (Kirby et al. 2015)	16.11	18.00

Note. Observables are taken from Martin et al. (2016b) unless otherwise noted.
[a]Distance from Tri II's centroid (Martin et al. 2016b) in arcseconds.
[b]Vizier online catalogue for GSC 2.3.2.

We have carried out an equivalent width (EQW) analysis of the spectrum of Star40, whereas the lower SNR for the spectrum of Star46 required us to rebin from R ~ 40 000 to ~20 000 and perform spectrum syntheses for only certain elements and iron. The synthetic line abundances for Star46 are listed in Table 3; note that the uncertainties in the synthetic fits per line are large due to uncertainties in the continuum placement, but vary with wavelength (0.2 < Δlog(X/H) < 0.5), with improved precision for lines at redder wavelengths and/or located in the centre of the echelle orders.

3 SPECTRAL ANALYSES

For Star40, the spectrum has sufficient SNR over enough of the wavelength range to carry out an abundance analysis. Line

[1] For more information on GRACES, see Chené et al. 2014, Pazder et al. 2014, or online at http://www.gemini.edu/sciops/instruments/graces/
[2] IRAF is distributed by the National Optical Astronomy Observatories, which are operated by the Association of Universities for Research in Astronomy, Inc., under cooperative agreement with the National Science Foundation.
[3] The OPERA pipeline does not currently adjust the slit tilt position.

Table 2. Stellar parameters.

Observable	Star40	Star46
RV (km s^{-1}, MJD2457373, this paper)	-382.1 ± 1.5	-397.1 ± 2.0^a
CaT RV (km s^{-1}, MJD2457302, Kirby et al. 2015)	-382.3 ± 1.5	-394.5 ± 1.7^a
CaT RV (km s^{-1}, MJD2457283, Martin et al. 2016b)	-379.2 ± 2.3	-372.5 ± 2.4^a
CaT [Fe/H] (Martin et al. 2016b)	-2.6 ± 0.1	-2.6 ± 0.1
CaT [Fe/H] (Kirby et al. 2015)	-2.86 ± 0.11	-2.04 ± 0.13
$T_{\rm eff}$ $(V-{\rm I})^b$	**4852**	**5069**
log g $(V-I)^b$	**1.84**	**2.63**
$T_{\rm eff}$ $(V-K)^c$	**4744**	–
log g $(V-K)^c$	**1.79**	–
$T_{\rm eff}$ $(V-I)^d$	4739	4954
log g $(V-I)^d$	1.81	2.62
$T_{\rm eff}$ $(V-I$; Kirby et al. 2015)	4922	5169
log g $(V-I$; Kirby et al. 2015)	1.88	2.74

Note. Stellar parameters have been determined using the colour–temperature relations for metal-poor red giants from Ramírez & Meléndez (2005; a comparison to Casagrande+2010 yields similar results). Stellar parameters using V, I and K magnitudes.

[a]The RV for Star46 in this paper is inconsistent with that reported from its CaT spectra. Careful analysis of the GRACES acquisition image assures us that it is the correct object, and similarly careful analysis of the OPERA data reduction pipeline suggests there is no unrecognized systematic error in the wavelength calibration (heliocentric corrections have been accounted for in the individual spectra before co-addition). We cannot account for these differences, unless perhaps this is a binary star.

[b] Photometry from $g_{\rm P1}r_{\rm P1}i_{\rm P1}$ with Tonry et al. (2012) conversions for V and I; see Table 1.

[c]Photometry from $g_{\rm P1}r_{\rm P1}i_{\rm P1}$ with Tonry et al. (2012) conversions for V and 2MASS K; see Table 1.

[d]Photometry from $g_{\rm P1}r_{\rm P1}i_{\rm P1}$ with Lupton (2005) conversions for V and I (see http://classic.sdss.org/dr4/algorithms/sdssUBVRITransform.html); see Table 1.

measurements for Star40 are listed in Table 3. Spectral lines have been selected from the line list described in Venn et al. (2012) in the analysis of metal-poor red giants in the Carina dwarf galaxy. The atomic data for these lines is primarily from the Kurucz data base,[4] updated with values in the National Institute of Standards and Technology data base,[5] and for Fe I lines when available from O'Brian et al. (1991). Hyperfine structure corrections for the Ba II and Eu II lines are taken from McWilliam (1998) and Lawler et al. (2001), respectively. For Star46, we rebin the spectrum to R$\sim$20 000 to reach SNR $\sim$ 20 and carry out spectrum synthesis only.

The effective temperature for the program stars was determined using the infrared flux method, following Ramírez & Meléndez (2005), and the photometry listed in Table 2. The $T_{\rm eff}$ values for Star40 were determined by averaging the $(V-I)$ and $(V-K)$ colour results (in bold in Table 2), using the $g_{\rm P1}r_{\rm P1}i_{\rm P1}$ data converted to V and I from the metal-poor star calibrations by Tonry et al. (2012). Uncertainties in $T_{\rm eff}$ due to photometric errors are negligible (<10 K), thus $\Delta T_{\rm eff} = \pm 50$ K is adopted from the difference in the colour values. Only the $(V-I)$ colour temperature was available for Star46, yet we adopt the same $T_{\rm eff}$ uncertainty as for Star40. Very similar results were determined using the calibrations by Casagrande et al. (2010).

A physical surface gravity was determined such that

$$\log g = 4.44 + \log(M_*) + 4\log(T_{\rm eff}/5780) + 0.4(M_{\rm bol} - 4.75).$$

A distance modulus $V_{\rm o} - M_{\rm V} = 17.40 \pm 0.14$ (Martin et al. 2016b; heliocentric distance of 30 kpc), and reddening[6] $E(B-V) = 0.07$, were adopted to determine the bolometric luminosity $M_{\rm bol}$ using the Ramírez & Meléndez (2005) calibrations. A stellar mass of $M_* = 0.8$ M$_\odot$ was assumed (typical for an old star from stellar isochrones), and the mean metallicity $\langle$[Fe/H]$\rangle = -2.60 \pm 0.2$ (Martin et al. 2016b) adopted throughout these calculations. The uncertainties in gravity, $\Delta \log g = 0.06$, are dominated by the error in the distance modulus.

Our stellar parameters differ from those adopted by Kirby et al. (2015) due to differences in both the photometry and methodology. They used Yonsei–Yale theoretical isochrones to fit their colours and magnitudes; with an initial estimate of [Fe/H] $= -1.5$ and a fixed log g, they determine $T_{\rm eff}$ and redetermine [Fe/H] by minimizing the differences between their CaT spectrum and those in a spectral grid described by Kirby et al. (2010). In general, their results are in good agreement with ours given the differences in our V and I magnitudes.

We compute elemental abundances using a recent version of the spectrum analysis code MOOG (Sneden 1973; Sobeck et al. 2011), which assumes local thermodynamic equilibrium (LTE) in the line-forming layers of the atmosphere, and adopting spherical MARCS model atmospheres (Gustafsson et al. 2008, further expanded by B. Plez). The initial step is to determine [Fe/H], microturbulence, and refine the temperature determination, from the individual Fe I spectral lines. An initial estimate for microturbulence was determined using the relationship with gravity for red giants by Marino et al. (2008); however, for Star40 this value proved to be too low since there are a sufficient number of individual Fe I lines for a direct measurement by flattening the slope in log(Fe I/H) versus the reduced equivalent widths (EQW/λ). For Star46, there are not enough Fe I lines over a range of excitation potentials and line strengths for a direct measure, thus an *offset* was determined from the gravity–microturbulence relationship relative to the value for Star40. The temperatures were checked by examining the slope in the Fe I abundances versus excitation potential (χ), but no adjustments were

[4] The Kurucz atomic and molecular database. [Online] Available at: http://kurucz.harvard.edu/LINELISTS/GFHYPERALL

[5] *NIST Atomic Spectra Database* (version 5.4): Kramida et al. (2016)

[6] The adopted reddening is between that of Schlafley & Finkbeiner (2011), $E(B-V) = 0.067$, and Schlegel, Finkbeiner & David (1998), $E(B-V) = 0.078$.

Table 3. Spectral lines and abundances.

Element	Wavelength (Å)	χ (eV)	log gf	STAR40 EQW (mÅ)	STAR40 logϵ(X/H)	STAR46 logϵ(X/H)
Fe I	4920.503	2.83	0.068	100	4.29	–
Fe I	4939.687	0.86	−3.252	74	4.88	–
Fe I	4957.610	2.81	0.233	100	4.10	–
Fe I	5006.120	2.83	−0.615	52	4.32	–
Fe I	5012.070	0.86	−2.642	101	4.63	–
Fe I	5041.072	0.96	−3.086	82	4.93	–
Fe I	5041.756	1.49	−2.203	105	5.01	–
Fe I	5049.820	2.28	−1.355	45	4.30	–
Fe I	5051.635	0.92	−2.764	104	4.86	–
Fe I	5123.720	1.01	−3.058	62	4.70	–
Fe I	5127.359	0.92	−3.249	50	4.63	–
Fe I	5131.470	2.22	−2.510	35	5.23	–
Fe I	5142.930	0.96	−3.080	91	5.03	–
Fe I	5150.850	0.99	−3.037	56	4.57	–
Fe I	5151.920	1.01	−3.321	65	4.99	–
Fe I	5166.280	0.00	−4.123	77	4.71	5.1
Fe I	5171.610	1.48	−1.721	113	4.61	4.6
Fe I	5192.340	3.00	−0.421	75	4.61	–
Fe I	5194.942	1.56	−2.021	92	4.70	4.6
Fe I	5198.710	2.22	−2.135	51	5.08	–
Fe I	5202.340	2.18	−1.838	70	4.98	–
Fe I	5204.580	0.09	−4.332	60	4.82	–
Fe I	5266.555	3.00	−0.385	61	4.39	–
Fe I	5269.537	0.86	−1.330	160	4.21	4.6
Fe I	5281.790	3.04	−0.833	40	4.59	–
Fe I	5283.621	3.24	−0.524	58	4.77	–
Fe I	5302.302	3.28	−0.880	30	4.75	–
Fe I	5324.190	3.21	−0.100	77	4.55	5.1
Fe I	5328.039	0.92	−1.465	184	4.77	5.1
Fe I	5328.530	1.56	−1.850	78	4.33	–
Fe I	5383.370	4.31	0.645	43	4.64	–
Fe I	5397.128	0.91	−1.980	112	4.13	4.6
Fe I	5405.775	0.99	−1.852	124	4.27	4.6
Fe I	5415.199	4.39	0.643	38	4.66	–
Fe I	5424.070	4.32	0.520	70	5.14	–
Fe I	5429.697	0.96	−1.881	135	4.43	4.0
Fe I	5434.524	1.01	−2.126	112	4.39	4.0
Fe I	5497.516	1.01	−2.825	89	4.77	5.1
Fe I	5501.465	0.96	−3.046	51	4.45	–
Fe I	5506.790	0.99	−2.789	93	4.76	4.6
Fe I	5572.842	3.40	−0.310	51	4.63	5.1
Fe I	5586.756	3.37	−0.144	82	4.84	–
Fe I	5615.660	3.33	0.050	70	4.43	4.6
Fe I	6136.615	2.45	−1.410	46	4.49	5.1
Fe I	6137.691	2.59	−1.346	37	4.47	–
Fe I	6230.740	2.56	−1.276	45	4.47	–
Fe I	6421.350	2.28	−2.014	40	4.79	5.1
Fe I	6430.846	2.18	−1.946	42	4.63	5.1
Fe I	6494.980	2.40	−1.239	53	4.33	5.4
Fe I	8327.056	2.20	−1.55	67	4.46	5.0
Fe I	8387.773	2.17	−1.51	73	4.45	5.0
Fe I	8468.407	2.22	−2.04	30	4.46	5.1
Fe II	4923.920	2.89	−1.320	111	4.70	–
Fe II	5018.430	2.89	−1.220	135	4.99	–
Fe II	5276.000	3.20	−1.950	40	4.67	–
Na I	5889.970	0.00	0.110	(S)	2.0	–
Na I	5895.924	0.00	−0.180	(S)	2.6	–
Na I	8183.255	2.10	0.230	(S)	<3.2	<3.7
Na I	8194.790	2.10	−0.470	(S)	<3.2	<3.7
Mg I	5172.700	2.71	−0.380	174	4.54	4.2
Mg I	5183.604	2.72	−0.160	191	4.55	4.2
Mg I	5528.410	4.34	−0.480	59	4.97	–

Table 3 – *Continued*

Element	Wavelength (Å)	χ (eV)	log gf	STAR40 EQW (mÅ)	STAR40 logϵ(X/H)	STAR46 logϵ(X/H)
Mg I	8806.756	4.34	−0.140	106	4.99	4.8
K I	7698.974	0.00	−0.170	(S)	4.2	–
Ca I	6102.730	1.88	−0.790	42	3.98	–
Ca I	6122.230	1.89	−0.320	79	4.00	3.4
Ca I	6162.173	1.90	−0.090	73	3.71	3.5
Ca I	6439.080	2.52	0.390	65	3.84	4.0
Ti I	5007.210	0.82	0.168	72	2.75	–
Ti I	5039.957	0.02	−1.130	57	2.89	–
Ti II	5154.070	1.57	−1.520	41	2.42	–
Ti II	5188.680	1.58	−1.220	72	2.53	–
Cr I	5208.419	0.94	0.160	84	2.23	–
Cr I	5409.800	1.03	−0.720	51	2.78	–
Ni I	6643.640	1.68	−2.30	(S)	3.80	–
Ni I	7714.340	1.68	−2.30	(S)	3.50	–
Ba II	6141.730	0.70	−0.077	(S, 1σ)	<−1.9	<−1.0
Ba II	6141.730	0.70	−0.077	(3σ)	<−1.3	<0.0
Eu II	6645.130	1.37	0.120	<20	<−0.5	–
Eu II	6645.130	1.37	0.120	(S)	<−1.1	–

Note. Spectral lines as described in Venn et al. (2012), where atomic data is primarily from the Kurucz data base, updated with values in the NIST data base, and further supplemented with atomic data for Fe I lines from O'Brian et al (1991) when available; see text.

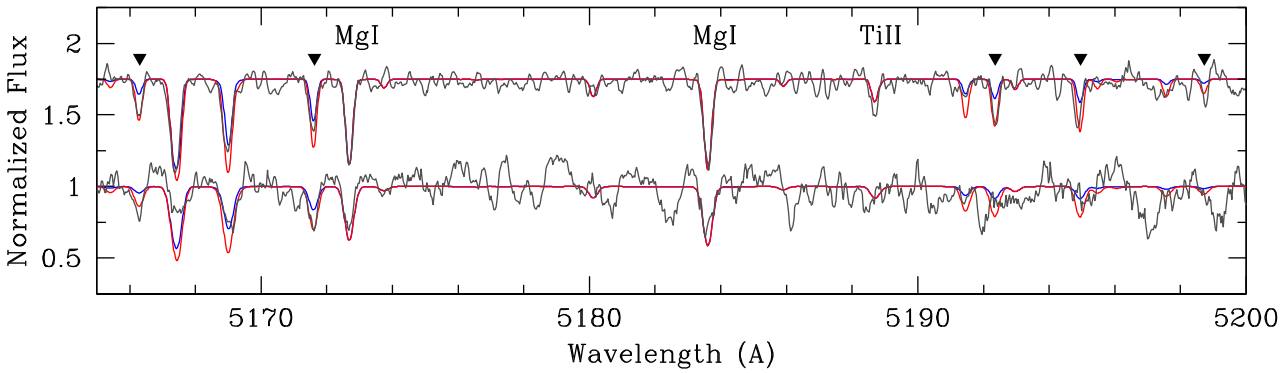

Figure 1. Spectrum synthesis in the Mgb region. All features used in the EQWs analysis of Star40 are marked (triangles with no labels indicates Fe I lines); fewer lines are used in the analysis of Star46 due to the poor SNR in this region (see Table 3). Red syntheses indicate the best fits from the EQWs analysis for Star40 (top spectrum), and the spectrum syntheses fits for Star46 (bottom spectrum). For illustration, a second fit for both stars with Δ[Fe/H] = −0.5 is shown in blue. The spectral region for Star40 is offset by +0.75 in flux for illustration.

necessary. Elemental abundances and EQWs from individual Fe I lines are in Table 3 for Star40. With very few Fe II lines in hand, ionization equilibrium was not used to refine the physical gravities.

Spectrum syntheses were carried out for certain wavelength regions to confirm the results for Star40 and estimate abundances for Star46 (in Table 3). These include: Mgb 5180 Å region (Fig. 1), Ca I and Ba II lines near 6100 Å (Fig. 2), CH features near 8400 Å (Fig. 3), Na I and CH features near 5000 Å (Fig. 4) and the Fe I abundances for Star46. Synthetic spectra are convolved with a Gaussian profile; for Star40 the full width at half-maximum (FWHM) = 0.2 Å, whereas for Star46 the broadening was higher with FWHM = 0.3 Å, due to our rebinning to increase the SNR.

Element abundance errors have been determined in two ways: (1) measurement errors are determined as the mean in the line scatter $\sigma/\sqrt{N}$, and (2) systematic errors are determined from the influence of the stellar parameter uncertainties. The latter are listed for both stars in Table 4. These systematic uncertainties are added in quadrature to one another and to the measurement errors for the total mean abundance errors listed in Table 5. These total mean abundances and errors are used throughout the discussion and in Fig. 5.

4 STELLAR ABUNDANCES

The [Fe/H] abundances for our two stars in Tri II are consistent with their CaT metallicity estimates (Kirby et al. 2015; Martin et al. 2016b), confirming that Tri II is a very metal-poor system.

Carbon: the CH molecular features near 8400 Å were examined in both stars (see Fig. 3) and near 5890 Å in Star40 (see Fig. 4). No features of CH are found, which provides upper limits on their carbon abundances. We find that these stars are not carbon-enhanced metal-poor stars (CEMP), showing [C/Fe] ≤−1.0 (See Table 5). At the metallicity of these stars ([Fe/H] > −3), a few CEMP stars are found in the dwarf galaxies (UMa II by Frebel et al. 2010b, Bootes I by Norris et al. 2010, Segue 1 by Norris et al. 2010 and Sculptor

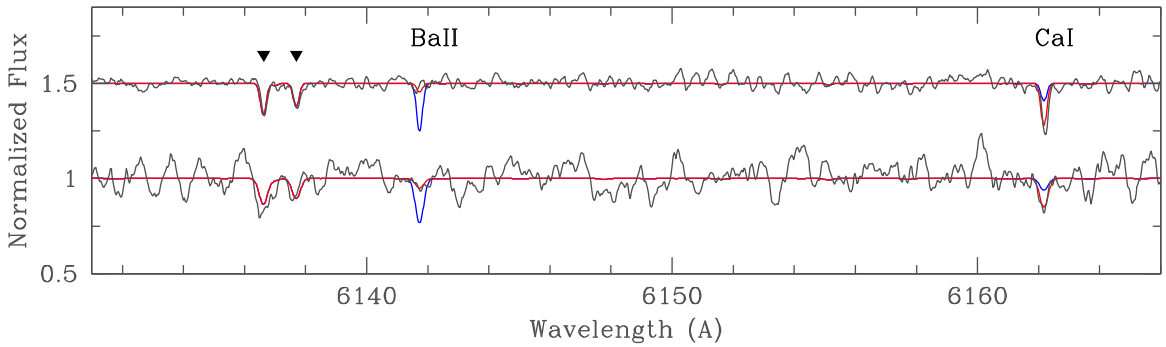

Figure 2. Spectrum synthesis of the Ba II and Ca I features near 6100 A (notice the significant improvement in the SNR of the spectra at this redder wavelength region than in Fig. 1). Red syntheses indicate the best fits from the EQWs analysis for Star40 (top spectrum), and the spectrum synthesis fits for Star46 (bottom spectrum). For illustration, a second fit for both spectra with Δ[Ca/Fe] $=-0.5$ and Δ[Ba/Fe]$=+1.0$ is shown in blue. The spectral region for Star40 is offset by $+0.75$ in flux for illustration.

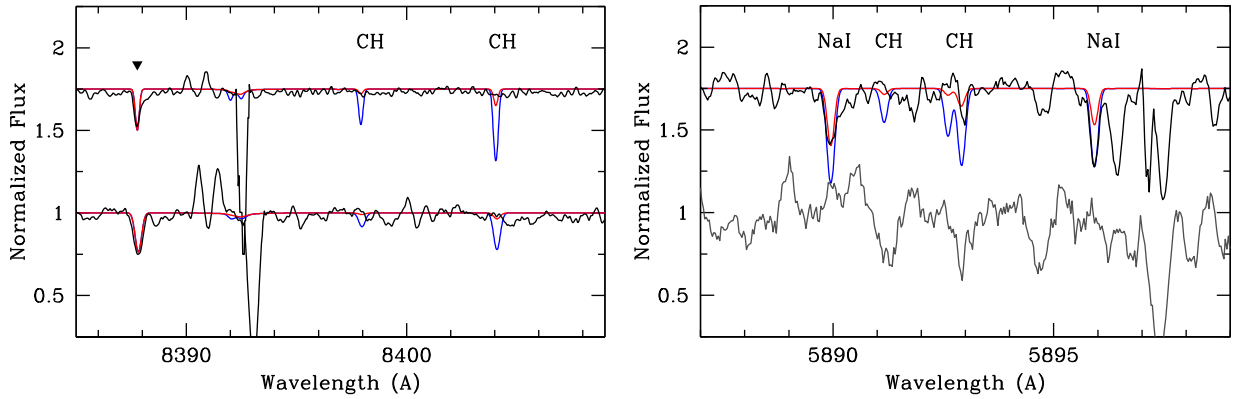

Figure 3. Left-hand panel: spectrum synthesis of the CH features near 8400 Å. Red syntheses indicate the best fits, where [C/Fe] $= -1.0$. For illustration, a second fit for both spectra with [C/Fe] $= 0.0$ is shown in blue. The imperfect sky subtraction in the two-fibre mode GRACES spectra can be seen near 8392 Å. Right-hand panel: spectrum syntheses of the NaD lines and CH features near 5890 Å in Star40 (the SNR for Star46 is too low). The best fits to Star40, with [C/Fe] $= -1.0$ and [Na/Fe] $= -1.4$ is shown in red, and [C/Fe] $= 0.0$ and [Na/Fe] $= -0.8$ in blue. We take the average for sodium, thus [Na/Fe] $= -1.1 \pm 0.3$. The imperfect sky subtraction in the two-fibre mode GRACES spectra can be seen near 5897 Å. In both panels, the spectral region for Star40 is offset by $+0.75$ in the flux for illustration.

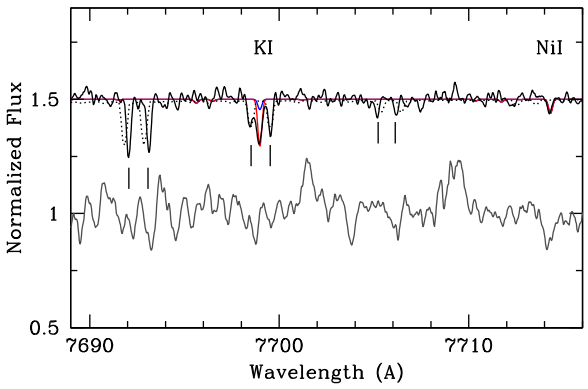

Figure 4. Spectrum syntheses of the K I feature in Star40, where [K/Fe] $= +0.8$ (red line) and [K/Fe] $= 0.0$ (blue line). Telluric lines near the K I feature are marked below the Star40 spectrum, and an imperfect theoretical estimate is shown (dotted line, from ESO SkyCalc, ESO Skycalc, based on the Cerro Paranal Sky Model by Noll et al. (2012) and Jones et al. (2013)). The spectral region for Star40 is offset by $+0.5$ in flux for illustration.

by Skuldottir et al. 2015) and these stars comprise 20–30 per cent of the Galactic halo (Yong et al. 2013; Placco et al. 2014).

Alpha-elements: these two stars in Tri II have low [Mg/Fe] and [Mg/Ca] values. Mg and Ca are well determined in Star40; however, spectrum synthesis was carried out for the Mgb lines near λ5200 (shown in Fig. 1) and the Mg I λ8807 in Star40; these results were averaged for the [Mg/Fe] ratio in Table 5. A larger uncertainty ($\sigma = 0.5$, $\sigma/\sqrt{3} = 0.3$) is adopted due to the poor quality of the Star46 spectrum and difficulty in placing the continuum. Even with this larger uncertainty, [Mg/Fe] appears to be truly lower in Star46 than the majority of stars at this metallicity (see Fig. 5). Even non-LTE corrections for these strong Mg lines is only expected to increase the [Mg/Fe] ratio by $\sim+0.2$ in these metal-poor giant atmospheres (Andrievsky et al. 2010). Similarly, spectrum syntheses are carried out for Ca I lines in Star46 (as shown in Fig. 2), and though these lines are weak, we are able to determine an abundance. The [Ca/Fe] abundance in Star46 is quite low; the large uncertainties in Mg and Ca in Star46 make it difficult to ascertain its [Mg/Ca] ratio, which could range from 0 (solar) to -1.0 (substantially subsolar). We also note that Star40 has high [Ti/Fe] from the average of two Ti I and two Ti II lines, in good agreement with its [Ca/Fe]. Both of these abundances have fairly small errors ($\sigma_{\rm TOT}$(Ti) ≤ 0.17) compared to that for Mg ($\sigma_{\rm TOT}$(Mg) $= 0.23$); this indicates that the

Table 4. Systematic abundance errors.

	σ/sqrt(N)	$\Delta T_{\rm eff}$ (+100 K)	$\Delta\log g$ +0.1	$\Delta\xi$ −0.5 km s^{-1}	Δ[Fe/H] −0.5
Star40					
[Fe I/H]	0.03	+0.13	0.00	+0.12	+0.03
[Fe II/H]	0.10	0.00	+0.03	+0.21	−0.04
[C/H]	–	−0.1	0.0	0.0	−0.2
[Na I/H]	0.3	+0.12	0.00	+0.20	+0.04
[Mg I/H]	0.13	+0.10	−0.01	+0.16	+0.03
[K I/H]	0.10	+0.10	+0.00	+0.13	+0.02
[Ca I/H]	0.06	+0.11	−0.01	+0.07	+0.02
[Ti/H]	0.05	+0.14	0.00	+0.08	+0.04
[Cr I/H]	0.28	+0.13	0.00	+0.09	+0.03
[Ni I/H]	0.20	+0.12	0.00	+0.06	+0.10
[Ba II/H]	–	+0.06	+0.04	+0.04	−0.06
[Eu II/H]	–	+0.03	+0.03	+0.01	−0.06
Star46					
[Fe I/H]	0.05	+0.16	+0.04	+0.12	+0.01
[C/H]	–	−0.1	0.0	0.0	−0.2
[Mg I/H]	0.3	+0.09	+0.01	+0.14	0.00
[Ca I/H]	0.3	+0.10	+0.02	+0.14	0.00
[Ba II/H]	–	+0.06	+0.04	+0.10	−0.05

Note. The impact on the average element abundances of 2σ uncertainties in the stellar parameters are listed here.

Table 5. Results for Tri II Star40 and Star46.

	Star40	Star46
$T_{\rm eff}$ (K)	4800 ± 50	5050 ± 50
log g (cgs)	1.80 ± 0.06	2.60 ± 0.06
ξ (km s^{-1})	2.7 ± 0.2	2.5
[Fe/H]	−2.87 ± 0.19 (55)	−2.5 ± 0.2 (21)
12+log(Fe I/H)	4.63 ± 0.19 (52)	5.0 ± 0.2 (21)
12+log(Fe II/H)	4.79 ± 0.24 (3)	–
[C/Fe]	<−1.0 (S)	<−1.0 (S)
[Na I/Fe]	−1.1 ± 0.4 (2)	<0.0 (S)
[Mg I/Fe]	0.01 ± 0.23 (4)	−0.7 ± 0.3 (3)
[K I/Fe]	+0.8 ± 0.2 (S)	–
[Ca I/Fe]	+0.39 ± 0.14 (5)	−0.2 ± 0.3 (3)
[Ti/Fe]	+0.55 ± 0.17 (4)	–
[Cr I/Fe]	−0.29 ± 0.32 (2)	–
[Ni I/Fe]	+0.30 ± 0.26 (2)	–
[Ba II/Fe]	<−1.2 (S)	<−0.7 (S)
[Ba II/Fe]	<−0.6 (3σ)	<+0.3 (3σ)
[Eu II/Fe]	<+1.9 (S)	–

Note. Elemental abundances are from both the EQW analysis and spectral syntheses results, both listed in Table 3. [X/Fe] = $\log(\rm X/Fe)_* - \log(\rm X/Fe)_\odot$, where the solar abundances are from Asplund et al. (2009). Abundance errors are conservatively estimated as the mean errors from the stellar parameter uncertainties and line-to-line scatter per element, added in quadrature.

lower Mg ratio in Star40 is real and of astrophysical interest (see Discussion below).

Odd-elements: sodium in Star40 is extremely low, with [Na/Fe] = −1.1 ± 0.3 (LTE). This does not reflect the Na–O anticorrelation, usually attributed to the formation of a second generation of stars in a globular cluster (e.g. Carretta et al. 2010). Corrections for non-LTE effects on the Na D resonance lines in our metal-poor red giant atmosphere could lower this to [Na/Fe] ≤−1.5 (NLTE, Andrievsky et al. 2007). We also examine the spectral region near λ8190 Å, but do not find the Na I subordinate lines; upper limits for both stars from these lines are near [Na/Fe] < 0. In addition, we are able to determine a potassium abundance in Star40. While both K I resonance lines are blended with features in the atmospheric *A* band, the line near λ7699 is sufficiently strong and isolated for a spectrum synthesis (see Fig. 4); the result from this fit is supported by the stronger but more blended K I feature near λ7665. The potassium abundance in Star40 is surprisingly large, e.g. compared to most stars in the field and globular clusters (Carretta et al. 2013), and even non-LTE corrections are only predicted to be ∼− 0.2 in [K/Fe] in these metal-poor red giant atmospheres (Andrievsky et al. 2010). We further discuss the high K and low Na (with low Mg) in Star40 in the Discussion section. Neither reliable determination nor upper limit is available for the K I line in Star46 (see Fig. 4).

Iron-group elements: very few lines have yet been analysed for the other iron-group elements in Star40; only two lines of Cr I and two line of Ni I. Both are in good agreement with [Fe/H], within their 1σ uncertainties.

Heavy elements: there are no heavy-element features observed in our spectra, yet the upper limits to the Ba II λ6141 line provide interesting constraints on the neutron-capture element abundances. For this reason, we determine the upper limits in two ways; matching the spectrum synthesis to the noise level and from the 3σ minimum EQW measurement as determined by the Cayrel (1988) formula (corrected as discussed in Venn et al. 2012). These two methods give upper limits in excellent agreement (see Fig. 5). Other Ba II lines (λ5853, λ6497) are also not present, and provide only weaker constraints, therefore are not used in this analysis. Follow-up high-SNR spectra at bluer wavelengths would test these limits further; in Fig. 5, the detection limits for the strongest Ba II 4554 Å line are shown for Star40 (T = 4800 K), a feature not available in our GRACES spectra.

Other elements: other elements (Li, Sc, Mn, Cu, Zn, Eu) were sought in Star40, and some upper limits were calculated, however none provided valuable constraints for examining the chemical evolution of these stars or this system.

5 DISCUSSION

Our analysis of the high-resolution Gemini/GRACES spectra of two stars in Tri II indicate that this low-mass system has similar properties to other faint dwarf galaxies discovered over the past decade. The Mg, Ca, Ba and Fe abundances of our two Tri II stars are compared to those published for stars in the Galactic halo, the Sculptor and Carina dwarf galaxies, and other faint dwarf galaxies in Fig. 5. The abundances for the Galactic halo stars are from the compilations gathered by Venn et al. (2004) and Frebel et al. (2010), and supplemented with targets from Reddy, Lambert & Allende Prieto (2006) and Yong et al. (2013). Data for stars in Sculptor are from Shetrone et al. (2003), Geisler et al. (2005), Tafelmeyer et al. (2010), Hill et al. (in preparation), Frebel et al. (2010), Starkenburg et al. (2013), Jablonka et al. (2015), Simon et al. (2015a) and Skuldottir et al. (2015). Carina stellar abundances are from Shetrone et al. (2003), Koch et al. (2008a), Venn et al. (2012), Lemasle et al. (2012) and 32 new stars by Norris et al. (in preparation). Elemental abundances are also shown for 11 ultrafaint dwarf galaxies including Bootes I (Feltzing et al. 2009; Norris et al. 2010; Ishigaki et al. 2014), Bootes II (Koch et al. 2014; François et al. 2015), Hercules (Koch et al. 2008b; Adén et al. 2011; Koch et al. 2013; François et al. 2016), Segue 1 (Frebel et al. 2014), Segue 2 (Roederer & Kirby 2014) Ursa Major II (Frebel et al. 2010b), Coma Berenices (Frebel et al. 2010b), Leo IV (Simon et al. 2010; François et al. 2016), Canes Venatici I and II (François et al. 2016) and Reticulum II (Ji et al. 2016; Roederer et al. 2016).

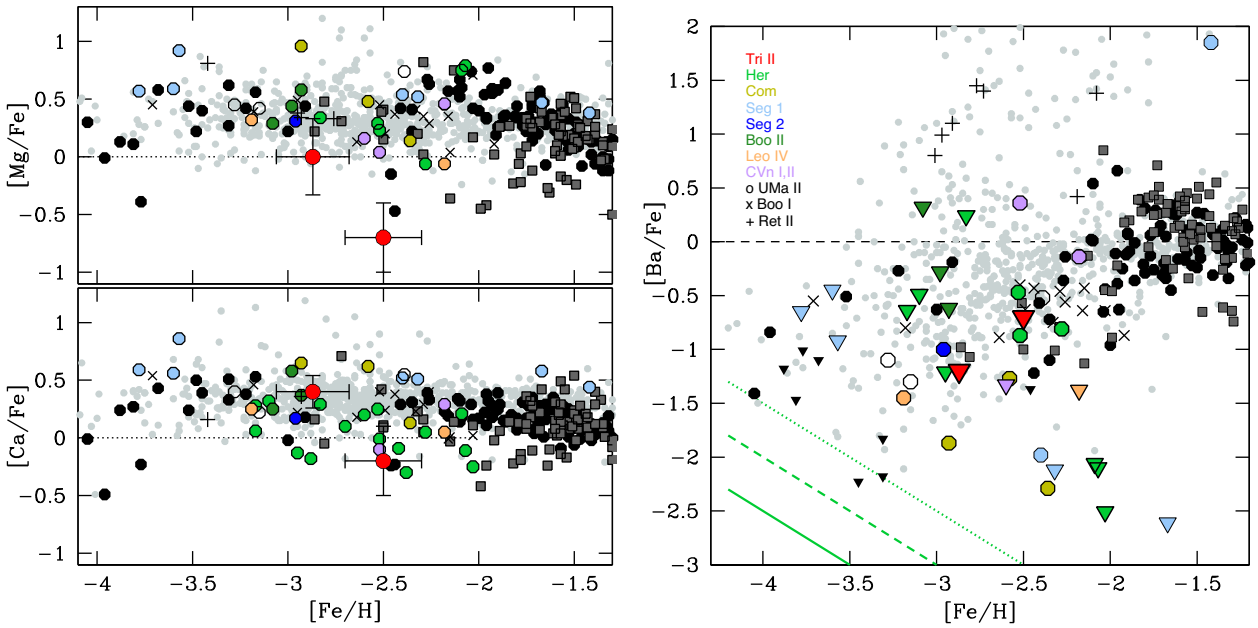

Figure 5. [Mg/Fe], [Ca/Fe] and [Ba/Fe] abundances in the two Tri II stars (red symbols with errorbars). For comparison, stars in the Galactic halo (light grey), Carina (grey filled squares) and Sculptor (black filled circles) dwarf galaxies, and several faint dwarf galaxies are shown (see legend). In the [Ba/Fe] plot, upper limits are shown as inverted triangles; upper limits for the two Tri II stars are shown in red. Detection limits for the strong Ba II λ4554 line in Star40 (T = 4800) are shown as green lines (dotted 10 mÅ, dashed 3 mÅ and solid 1 mÅ).

5.1 Comparing Tri II to other dwarf galaxies

Dwarf galaxies are outstanding laboratories for examining variations in the early chemical evolution of the Universe and testing the yields from low-metallicity stars. Frebel & Norris (2015) show that if one assumes an average iron yield from a core collapse SNe II to be 0.1 $M_\odot$ (e.g. Heger & Woosley 2010) and this is homogeneously and instantaneously mixed into a pristine star-forming cloud of 10^5 $M_\odot$, then the resulting metallicity of this cloud is [Fe/H] = −3.2. Thus, stars with [Fe/H] ∼ −3 in the ultrafaint, low-mass, dwarf galaxies could be second generation stars, whose chemical abundances reflect the yields from only one (or a few) SNe II. Subsampling of the upper initial mass function (IMF) and inhomogeneous mixing of those stellar yields can also be studied in the chemical evolution of these systems. Of course, this assumes that all of the metals are retained in these dwarf galaxies when calculating [Fe/H] and the abundance ratios, which is difficult to reconcile with the high rates of metal losses predicted in the simple chemical evolution scenarios, as shown by Kirby, Martin & Finlator (2011). In our discussion, we assume that these mass-loss events do not alter the chemical abundance *ratios* of these systems, even if they lower the overall yields from each SN II event.

Our abundances of [Ca/Fe] and [Ba/Fe] in Tri II resemble the distribution seen in Hercules, as examined by Koch et al. (2008b, 2013) and Adén et al. (2011); see Fig. 5. Koch et al. (2013) used stellar yields for Pop III stars from Heger & Woosley (2010) to estimate that only one to three SNe II with progenitor masses <30 $M_\odot$ could account for the mean Fe and Ca abundances while ejecting little to no Ba. They further showed that an examination of chemical evolution models by Lanfranchi & Matteucci (2004) can be consistent with the abundance *distribution* in Hercules. Thus, Hercules can be explained by a very low star formation rate, where star formation was extended over time (time delay model) to keep *s*-process contributions to Ba low, while SNe Ia slowly contributed to the buildup of Fe (and with minor decreases in [Ca/Fe] as seen). Thus, the chemical composition of Hercules can be explained as a natural consequence of the time delay model but with a very low star formation rate.

The time delay model also applies to the more massive classical dwarf galaxies, e.g. Carina[7] and Sculptor (e.g. Tolstoy et al. 2009; Vincenzo et al. 2014), also shown in Fig. 5. In those dwarf galaxies, the nucleosynthesis of the individual alpha-elements need not to be scaled together, as in the Galaxy, due to differences in their star formation histories (also see de Boer et al. 2012, 2014; Revaz & Jablonka 2012). The low [Mg/Fe] ratios in Carina have been interpreted in terms of the chemical evolution of this galaxy, either through inhomogeneous contributions to Fe from SNe Ia or fewer high-mass stars contributing Mg as Fe increases (Lemasle et al. 2012; Venn et al. 2012; de Boer et al. 2014). In Sculptor, the star formation history is somewhat simpler and the distribution in [Mg/Fe] and [Ca/Fe] is interpreted simply as contributions from SNe Ia (de Boer et al. 2012; Vincenzo et al. 2014; Jablonka et al. 2015). Inhomogeneous mixing is again indicated in both dwarf galaxies, by the dispersion in the Mg, Ca and Ba ratios at intermediate metallicities, which is also seen in our two Tri II stars.

On the other hand, Segue 1 cannot be explained by the time delay model. The alpha-element abundances (Mg, Ca, Ti) as determined by Frebel et al. (2014) are clearly enhanced at all metallicities in Segue 1 (up to [Fe/H] = −1.5), while the neutron-capture elements are low; in fact, [(Sr,Ba)/H] are flat,[8] showing no enhancements with

[7] We note that two stars in Carina have been reported with extremely low Mg abundances ([Mg/Fe]∼− 2.0) by Lemasle et al. (2012) from low SNR, high-resolution ESO FLAMES/UVES spectroscopy (see Pasquini et al. 2002). A reanalysis of those two stars by Fabrizio et al. (2015) and Norris et al. (in preparation) does not reproduce such extremely low Mg in those two stars, instead [Mg/Fe]∼− 0.8.

[8] Note, we cannot measure Sr in our stars because all of the Sr II spectral lines are at bluer wavelengths than available in our spectra.

metallicity This abundance distribution pattern is more consistent with inhomogeneous mixing of the gas *and* stochastic sampling of the SNe II yields (e.g. Greif et al. 2010; Wise et al. 2012; Kobayashi et al. 2014), e.g. one-shot enrichment by a massive SNe II with no subsequent chemical evolution. Simon et al. (2010) suggest a similar scenario for Leo IV based on the chemical abundances of one star; however, the recent analysis of a second less metal-poor star by François et al. (2016) shows that it has lower [(Mg and Ca)/Fe] and possibly lower [Ba/Fe] (upper limit only; see Fig. 5). Thus, this puts Segue 1 in a special class of the ultrafaint dwarf galaxies. In addition to its chemistry, its total luminosity is very close to that predicted by Bovill & Ricotti (2011) from simulations for the lowest mass primordial galaxies. Frebel & Norris (2015) suggest Segue 1 is 'most likely the most primitive galaxy known'.

These two Tri II stars do appear to have distinctively different metallicities; however, the higher metallicity star could be consistent with inhomogeneous mixing in the one-shot enrichment model (like Segue 1), *or* with the time delay model with a very slow star formation rate (like Hercules). Thus, while Tri II is clearly a faint system based on its luminosity (log (L_V/L$_\odot$ = 2.6 ±0.2, Kirby et al. 2015), it is not yet possible to identify it as a primordial galaxy, i.e. one that has undergone *chemical enrichment only* from one that has undergone *chemical evolution* (and may have been larger in the past). Solid detections of the Ba II lines and precise [Ba/Fe] abundances could distinguish these two cases, where the one-shot enrichment model predicts much lower [Ba/Fe] values; unfortunately, we only have upper limits for both stars.

As a final note, the only faint dwarf galaxy that Tri II does *not* resemble is Ret II, primarily due to the very high neutron-capture ratios that have been found in the Ret II stars. These high ratios are attributed to homogeneous enrichment by a single rare event, such as a compact binary merger (Ji et al. 2016; Roederer et al. 2016). This is an exciting system in terms of understanding the nucleosynthesis of *r*-process elements; however, the processes in this system are not similar to those that enriched our two stars in Tri II .

5.2 Is Tri II a primordial dwarf galaxy?

Frebel & Bromm (2012) considered the chemical signatures expected in a primordial galaxy, a first galaxy that experienced a Pop III generation plus one additional first generation of Pop II stars (formed from somewhat metal-enriched gas) before losing its gas and the possibility for subsequent star formation. The Pop II generation would include low-mass, long-lived stars with the chemical make-up of a galaxy with a heavily truncated star formation history. In this case, they suggest that such a system would have (1) a large spread in [Fe/H], with a low average metallicity and the existence of stars with [Fe/H] < -3, (2) a halo-like chemical abundance distribution similar to that of SNe II enrichments, (3) no signs of asymptotic giant branch (AGB) enrichments in the neutron-capture elements and (4) no downturn in [α/Fe] at higher metallicities ([Fe/H] > -2) due to the onset of iron-producing SNe Ia.

Our results for these two stars in Tri II are in agreement with point (3), and marginally in agreement with points (1), (2) and (4). Regarding point (1), we have not found stars with [Fe/H] < -3, and our metallicity spread is only Δ[Fe/H] $\sim 2\sigma$; Martin et al. (2016b) suggest the metallicity spread could be larger based on their CaT analysis. Regarding point (2), our [Ca/Fe] abundances are in agreement with the range seen for stars in the halo; however, our [Mg/Fe] abundances and [Na/Fe] upper limit for Star40 are lower. Low [Mg/Ca] could indicate stochastic sampling of the upper IMF which is unlike the halo, e.g. chemical yields from a single (or few) massive SNe II that produce more Ca than Mg.[9] However, regardless of the specifics of the SNe II progenitor(s), stochastic sampling of few massive SNeII in Tri II could still indicate that this is a pristine dwarf galaxy. Regarding point (4), our highest metallicity star at [Fe/H] $= -2.7$ has lower [Mg/Fe] and [Ca/Fe] than our lowest metallicity star (though only at the 1σ–2σ level). This might hint at a knee in [α/Fe], though this knee would be at [Fe/H] ≤ -2.7. This is much lower than that estimated by Frebel & Bromm (2012), as well as the minimum metallicity for AGB contributions estimated by Simmerer et al. (2004). If metal-poor SNe Ia and AGB stars have contributed to the gas that formed the higher metallicity star (Star46) then we may see a rise in its [Ba/Fe] compared with Star40. Unfortunately, we have only determined upper limits to Ba in both stars. We cannot examine the distribution in the Ba abundances, and therefore we cannot clearly identify Tri II as a primitive galaxy based on only these observations. Observations of the blue Ba II λ4554 line at very high-SNR data would provide a better constraint than currently available from our Gemini/GRACES spectra ($\lambda > 5000$ Å), based on predictions shown in Fig. 5. Observations of the Eu II λ4129 line would also be important for interpreting the neutron-capture ratios in this system in terms of *r*-process and *s*-process contributions.

5.3 Is Tri II similar to NGC 2419?

The outer halo globular cluster NGC 2419 has a unique chemical signature that has been found nowhere else in the Galaxy. Cohen, Huang & Kirby (2011) first noticed that this cluster has a few stars that are very poor in Mg, but rich in K, with no other significant chemical anomalies, nor spread in metallicity. Cohen & Kirby (2012) and Mucciarelli et al. (2012) confirmed these results, and the latter further suggested that ∼40 per cent of their sample could have subsolar [Mg/Fe] with enriched [K/Fe]. Neither group could find a nucleosynthetic source for these anomalies, nor could these be attributed to atmospheric effects or spectroscopic measurement errors. The uniqueness of this chemical signature has been further emphasized by the lack of stars with these chemical abundances in other normal globular clusters or the field (Carretta et al. 2013), although Mucciarelli et al. (2015) suggest a weak signature could be present in NGC 2808.

In this paper, both Star40 and Star46 have low [Mg/Fe] abundances. To compare these stars to NGC 2419, we searched for the K I λ7699 line, and found it between weak telluric features in Star40 (see Fig. 4). A comparison of the [Mg/Fe] and [K/Fe] abundances in NGC 2419 and our two stars in Tri II is shown in Fig. 6.

Ventura et al. (2012) suggested that high-temperature (well above 10^8 K) hydrogen-burning could account for these abundance anomalies, possibly in super-AGB stars (those near 8 M$_\odot$). Recently, Iliadis et al. (2016) confirm these predictions and suggest another site could be low metallicity nova, involving either a CO or ONe white dwarf. Iliadis et al. also predict that high-temperature H-burning would affect O, Na, Al, and to a lesser extent C, lowering each of these abundances while enriching K. Cohen & Kirby (2012) do not find low [Na/Fe] in their Mg-poor/K-rich stars, and Mucciarelli et al. (2012) do not report Na abundances. However, in our Star40 analysis, we do find low Na, low Mg and enriched K, consistent with the predictions from Iliadis et al. (2016).

[9] Some SNe II models with masses of 10–12 or 20–22 M$_\odot$ and standard mixing produce Ca > Mg (Woosley & Weaver 1995; Heger & Woosley 2010).

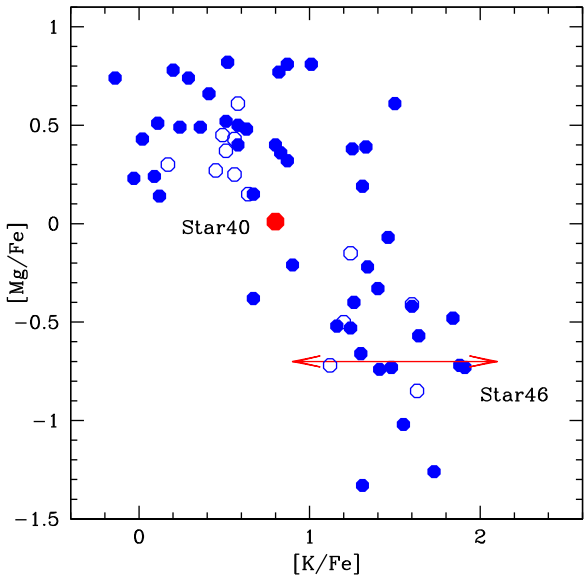

Figure 6. Comparison of [Mg/Fe] and [K/Fe] abundances in our two Tri II stars to those in the peculiar outer halo globular cluster NGC 2419. We cannot constrain the [K/Fe] abundance in Star46. Data are taken from Mucciarelli et al. (2012; solid blue circles) and Cohen & Kirby (2012; empty blue circles).

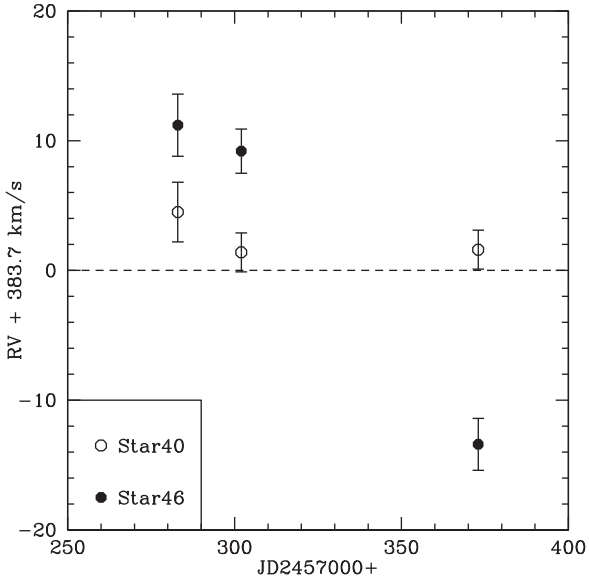

Figure 7. Radial velocities of Star40 and Star46, relative to the mean RV $v_{\rm rad} = -383.7\,{\rm km\,s^{-1}}$ of Tri II (Martin et al. 2016b).

5.4 Binarity of Star46

Star46 appears to have undergone a change in its RV in 2015. As shown in Fig. 7, it has changed by 24.6 km s^{-1}, approximately 12× larger than the mean measurement errors of only 2.1 km s^{-1}, over 103 d (2015 September 17 to December 17). Koch et al. (2014) have monitored an RV variable in Hercules (Her-3) and determined an orbital period $P = 135$ d, with maximum semi-amplitude $K = 15.2\,{\rm km\,s^{-1}}$, and ellipticiy $e = 0.18$. Though we have only three measurements for Star46, it is consistent with the variations seen in Her-3. Analysis of five red giants in Segue 1 (Simon et al. 2011) also showed that one is in a binary system, with a change in RV ∼ 13 km s^{-1}and orbital period ∼1 yr. Segue 1 has one additional star that is clearly in a binary system but did not show significant RV variations; Frebel et al. (2014) show that SDSS J100714+160154 is a CH star, with evidence for mass transfer from an AGB in a binary system resulting in enrichments in carbon, Sr and Ba via the *s*-process, and even the detection of Pb. A similar analysis of variability in Bootes I (Koposov et al. 2011) found binary stars with similar velocity variations over similar periods (see their fig. 10). These values are also consistent with variations typical of the CEMP-s stars (Lucatello et al. 2005; Starkenburg et al. 2014), even though our stars in Tri II are not carbon rich (Table 5), thus do not show signs of having received material in a binary companion.

Koch et al. (2014) discuss whether short-term binary orbits may directly inhibit *s*-process production and chemical evolution of neutron-capture elements in a faint dwarf galaxy. When *s*-process production occurs in AGB stars, then AGB stars that are in binary systems could have their outer layers removed during the common envelope phase, thereby preventing thermal pulsing and the third dredge-up (McCrea 1964; Izzard et al. 2006; Lau, Stancliffe & Tout 2008, 2009). In low-mass, low-metallicity systems, this could have a significant impact on the [Ba/Fe] ratios observed in stars. For Hercules, Koch et al. (2013) examined [Ba/Fe] in 11 stars and found that they all have low [Ba/Fe], which implies that all AGB stars would have been in close binaries and that they all had their outer envelopes removed to inhibit all *s*-process production in this dwarf galaxy. They conclude that this is an unlikely scenario for an entire system; on the other hand, Tri II has even fewer stars, which increases the likelihood of a global suppression. More precise [Ba/Fe] measurements, or other neutron-capture element abundances, would be necessary to test this hypothesis further.

Examination of the binary fractions in ultrafaint dwarf galaxies has shown that systems do tend to have a significant number of stars in binary systems (Koposov et al. 2011; Simon et al. 2011; Geha et al. 2013). This does not differ significantly from FGK stars in the Galaxy (Raghavan 2010) nor K dwarfs in the solar neighbourhood (Duquennoy & Mayor 1991); however, this can have a significant impact on the *M*/*L* determinations of the small systems by potentially inflating the apparent velocity dispersion (see McConnachie & Cote 2010). In the case of Tri II, though, the binarity of Star46 has had little impact on the *previous M*/*L* ratio calculations – its RV from the 2015 CaT studies was in the mean, not in the high-velocity tail, as in our GRACES spectra. Removing this one star from the previous calculations has no significant impact on the velocity dispersion; with Star46, $\sigma(v_r) = 10.1$ (+3.3/−2.5) km s^{-1}(Martin et al. 2016b), whereas without Star46 it is 9.9 (+3.2/−2.5) km s^{-1}. Of course, this does not rule out that other stars in the high-velocity tail of those calculations are also binaries.

6 SUMMARY AND CONCLUSIONS

In this paper, we determine the radial velocities and chemical abundance patterns of the two brightest (RGB) stars in Tri II, a faint dwarf galaxy originally discovered in the Pan-STARRS 1 Survey (Laevens et al. 2015) and spectroscopically confirmed to be dynamically hot, dynamically complex, and with evidence for a metallicity dispersion (Kirby et al. 2015; Martin et al. 2016b). To achieve this goal, we obtained high-resolution spectra with the new Gemini GRACES capability for Star40 and Star46. Our detailed model atmospheres analysis improves the individual [Fe/H] measurements, and we find that Star40 and Star46 have different metallicities, at the 2σ level. We determine [X/Fe] ratios for Mg and Ca in both stars, as well as results or upper limits for C, Na, K, Ti, Cr, Ni, Ba and Eu. Overall, the chemical abundances in these two stars are similar to those of

similar metallicity stars in the Galactic halo, with the exception of low [Mg/Fe] in both stars, a lower [Ca/Fe] in Star46 and a low [Na/Fe] upper limit in Star40. Star40 also shows an enhancement in [K/Fe], similar to stars in the unique outer halo globular cluster NGC 2419. We also note that Star46 is in a binary system, having undergone a change in its RV in 2015; however, there is no evidence for mass transfer in this binary system (e.g. [C/Fe] <-1), and removing this star has no significant impact on the previous determination of the velocity dispersion in Tri II.

When the chemistry of these two stars in Tri II are compared with stars in the faint dwarf galaxies, the distributions in Mg, Ca and Na are similar to Hercules, Carina and Sculptor. Each of those galaxies is expected to have undergone simple time delay chemical evolution, however we cannot confirm whether Tri II has also experienced chemical evolution, or a one shot chemical enrichment episode. For example, both stars have [Fe/H] > -3, and our higher metallicity star has lower [Mg/Fe], but both stars have quite low [Mg/Ca]. This pattern could be consistent with the predictions from either model. Determination of the Ba and Eu abundances from higher SNR spectra at bluer wavelengths would help to differentiate these models and identify whether Tri II is a remnant of a primitive galaxy.

Facilities: Gemini-GRACES

ACKNOWLEDGEMENTS

Our thanks to Andreas Koch and the anonymous referee for helpful comments that have improved this paper. Based on observations obtained with ESPaDOnS, located at the Canada-France-Hawaii Telescope (CFHT). CFHT is operated by the National Research Council of Canada, the Institut National des Sciences de l'Univers of the Centre National de la Recherche Scientique of France, and the University of Hawai'i. ESPaDOnS is a collaborative project funded by France (CNRS, MENESR, OMP, LATT), Canada (NSERC), CFHT and ESA. ESPaDOnS was remotely controlled from the Gemini Observatory, which is operated by the Association of Universities for Research in Astronomy, Inc., under a cooperative agreement with the NSF on behalf of the Gemini partnership: the National Science Foundation (United States), the National Research Council (Canada), CONICYT (Chile), Ministerio de Ciencia, Tecnología e Innovación Productiva (Argentina) and Ministério da Ciência, Tecnologia e Inovação (Brazil). We are grateful to the Gemini Observatory Director Markus Kissler-Patig for the opportunity to obtain Gemini/GRACES spectra for these stars through the Director's Discretionary Time program. We would also like to thank Andre-Nicolas Chené for his expert help with GRACES. ES gratefully acknowledges funding by the Emmy Noether program from the Deutsche Forschungsgemeinschaft (DFG). BPML gratefully acknowledges support from FONDECYT postdoctoral fellowship No. 3160510. KV acknowledges research support from the NSERC Discovery Grants program.

REFERENCES

Adén D., Eriksson K., Feltzing S., Grebel E. K., Koch A., Wilkinson M. I., 2011, A&A, 525, 153
Andrievsky S. M., Spite M., Korotin S. A., Spite F., Bonifacio P., Cayrel R., Hill V., François P., 2007, A&A, 464, 1081
Andrievsky S. M., Spite M., Korotin S. A., Spite F., Bonifacio P., Cayrel R., François P., Hill V., 2010, A&A, 509, 88
Asplund M., Grevesse N., Sauval A. J., Scott P., 2009, ARA&A, 47, 481
Bechtol K. et al., 2015, ApJ, 807, 50
Belokurov V., 2013, New Astron. Rev., 57, 100
Bovill M. S., Ricotti M., 2011, ApJ, 741, 18
Bullock J. S., Stewart K. R., Kaplinghat M., Tollerud E. J., Wolf J., 2010, ApJ, 717, 1043
Carretta E., Bragaglia A., Gratton R. G., Recio-Blanco A., Lucatello S., D'Orazi V., Cassisi S., 2010, A&A, 516, A55
Carretta E., Gratton R. G., Bragaglia A., D'Orazi V., Lucatello S., Sollima A., Sneden C., 2013, ApJ, 769, 40
Casagrande L., Ramírez I., Meléndez J., Bessell M., Asplund M., 2010, A&A, 512, 54
Cayrel R., 1988, in Cayrel de Strobel G., Spite M., eds, IAU Symp. 132, The Impact of Very High S/N Spectroscopy on Stellar Physics. Kluwer, Dordrecht, p. 345
Chené A. N. et al., 2014, in Navarro R., Cunningham C. R., Barto A. A., eds, Proc. SPIE Conf. Ser. Vol. 9151, Advances in Optical and Mechanical Technologies for Telescopes and Instrumentation. SPIE, Bellingham, p. 47
Cohen J. G., Kirby E. N., 2012, ApJ, 760, 86
Cohen J. G., Huang W., Kirby E. N., 2011, ApJ, 740, 60
de Boer T. J. L. et al., 2012, A&A, 539, 103
de Boer T. J. L., Tolstoy E., Lemasle B., Saha A., Olszewski E. W., Mateo M., Irwin M. J., Battaglia G., 2014, A&A, 572, 10
Donati J. F., 2003, in Trujillo-Bueno J., Almeida J. S., eds, ASP Conf. Ser. Vol. 41, Solar Polarization. Astron. Soc. Pac., San Francisco, p. 41
Drlica-Wagner A. et al., 2015, ApJ, 813, 109
Duquennoy A., Mayor M., 1991, A&A, 248, 485
Faber S. M. et al., 2003, SPIE, 4841, 1657
Fabrizio M. et al., 2015, A&A, 580, 18
Feltzing S., Eriksson K., Kleyna J., Wilkinson M. I., 2009, A&A, 508, L1
François P., Monaco L., Bonifacio P., Moni Bidin C., Geisler D., Sbordone L., 2016, A&A, 588, A7
Frebel A., Bromm V., 2012, ApJ, 759, 115
Frebel A., Norris J. E., 2015, ARA&A, 53, 631
Frebel A., Kirby E. N., Simon J. D., 2010a, Nature, 464, 72
Frebel A., Simon J. D., Geha M., Willman B., 2010b, ApJ, 708, 560
Frebel A., Simon J. D., Kirby E. N., 2014, ApJ, 786, 74
Geha M., Willman B., Simon J. D., Strigari L. E., Kirby E. N., Law D. R., Strader J., 2009, ApJ, 692, 1464
Geha M. et al., 2013, ApJ, 771, 29
Geisler D., Smith V. V., Wallerstein G., Gonzalez G., Charbonnel C., 2005, AJ, 129, 1428
Geringer-Sameth A., Koushiappas S. M., Walker M. G., 2015, Phys. Rev. D, 91, 3535
Gilmore G., Norris J. E., Monaco L., Yong D., Wyse R. F. G., Geisler D., 2013, ApJ, 763, 61
Greif T. H., Glover S. C.O, Bromm V., Klessen R. S., 2010, ApJ, 716, 510
Gustafsson B., Edvardsson B., Eriksson K., Jørgensen U. G., Nordlund Å., Plez B., 2008, A&A, 486, 951
Hargis J. R. et al., 2014, ApJ, 818, 39
Hayashi K., Ichikawa K., Matsumoto S., Ibe M., Ishigaki M. N., Sugai H., 2016, MNRAS, 461, 2914
Heger A., Woosley S. E., 2010, ApJ, 724, 341
Iliadis C., Karakas A. I., Prantzos N., Lattanzio J. C., Doherty C. L., 2016, ApJ, 818, 98
Ishigaki M. N., Aoki W., Arimoto N., Okamoto S., 2014, A&A, 562, 146
Izzard R. G., Dray L. M., Karakas A. I., Lugaro M., Tout C. A., 2006, A&A, 460, 565
Jablonka P. et al., 2015, A&A, 583, 67
Ji A. P., Frebel A., Chiti A., Simon J. D., 2016, Nature, 531, 610
Jones A., Noll S., Kausch W., Szyszka C., Kimeswenger S., 2013, A&A, 560, A91
Kim D., Jerjen H., 2015, ApJ, 808, 39
Kirby E. N. et al., 2010, ApJS, 191, 352
Kirby E. N., Martin C. L., Finlator K., 2011, ApJ, 742, L25
Kirby E. N., Boylan-Kolchin M., Cohen J. G., Geha M., Bullock J. S., Kaplinghat M., 2013, ApJ, 770, 16
Kirby E. N., Cohen J. G., Simon J. D., Guhathakurta P., 2015, ApJ, 814, 7
Kobayashi C., Ishigaki M. N., Tominaga N., Nomoto K., 2014, ApJ, 785, 5

Koch A., Grebel E. K., Gilmore G. F., Wyse R. F. G., Kleyna J. T., Harbeck D. R., Wilkinson M. I., Wyn Evans N., 2008a, AJ, 135, 1580
Koch A. et al., 2008b, ApJ, 658, 13
Koch A. et al., 2009, ApJ, 690, 453
Koch A., Feltzing S., Adén D., Matteucci F., 2013, A&A, 554, 5
Koch A., Hansen T., Feltzing S., Wilkinson M.I, 2014, ApJ, 780, 91
Koposov S. E. et al., 2011, ApJ, 736, 146
Koposov S. E. et al., 2015, ApJ, 811, 62
Kramida A., Ralchenko Yu., Reader J., the NIST ASD Team, 20l6, [Online]. Available at: http://physics.nist.gov/asd
Laevens B. P. M. et al., 2015, ApJ, 802, 18
Lanfranchi G. A., Matteucci F., 2004, MNRAS, 351, 1338
Lau H. H. B., Stancliffe R. J., Tout C. A., 2008, MNRAS, 385, 301
Lau H. H. B., Stancliffe R. J., Tout C. A., 2009, MNRAS, 396, 1046
Lawler J. E., Wickliffe M. E., den Hartog E. A., Sneden C., 2001, ApJ, 563, 1075
Lemasle B. et al., 2012, A&A, 538, 100
Lucatello S., Tsangarides S., Beers T. C., Carretta E., Gratton R. G., Ryan S. G., 2005, ApJ, 625, 825
Lupton R. H. et al., 2005, BAAS, 37, 1384
McConnachie A. W., 2012, AJ, 144, 4
McConnachie A. W., Cote P., 2010, ApJ, 722, 209
McCrea W. H., 1964, MNRAS, 128, 147
McWilliam A., 1998, AJ, 115, 1640
Marino A. F., Villanova S., Piotto G., Milone A. P., Momany Y., Bedin L. R., Medling A. M., 2008, A&A, 490, 625
Martin N. F. et al., 2016a, MNRAS, 458, 59
Martin N. F. et al., 2016b, ApJ, 818, 40
Martioli E., Teeple D., Manset N., Devost D., Withington K., Venne A., Tannock M., 2012, in Radziwill N. M., Chiozzi G., eds, Proc. SPIE Conf. Ser. Vol. 8451, Software and Cyberinfrastructure for Astronomy II. SPIE, Bellingham, p. 84512B
Mucciarelli A., Bellazzini M., Ibata R., Merle T., Chapman S. C., Dalessandro E., Sollima A., 2012, MNRAS, 426, 2889
Mucciarelli A., Lapenna E., Massari D., Pancino E., Stetson P. B., Ferraro F. R., Lanzoni B., Lardo C., 2015, ApJ, 809, 128
Noll S., Kausch W., Barden M., Jones A. M., Szyszka C., Kimeswenger S., Vinther J., 2012, A&A, 543, A92
Norris J. E., Wyse R. F. G., Gilmore G., Yong D., Frebel A., Wilkinson M. I., Belokurov V., Zucker D. B., 2010, ApJ, 723, 1632
O'Brian T. R., Wickliffe M. E., Lawler J. E., Whaling W., Brault J. W., 1991, J. Opt. Soc. Am. B, 8, 1185
Pasquini L. et al., 2002, The Messenger, 110, 1
Placco V. M., Frebel A., Beers T. C., Stancliffe R. J., 2014, ApJ, 797, 21
Pazder J., Fournier P., Pawluczyk R., van Kooten M., 2014, Proc. SPIE, 9151, 24
Raghavan D., 2010, ApJS, 190, 1
Ramírez I., Meléndez J., 2005, ApJ, 626, 446
Reddy B. E., Lambert D. L., Allende Prieto C., 2006, MNRAS, 367, 1329
Revaz Y., Jablonka P., 2012, A&A, 538, 82
Roederer I. U., Kirby E. N., 2014, MNRAS, 440, 2665
Roederer I. U. et al., 2016, AJ, 151, 82
Schlafley E. G., Finkbeiner D. P., 2011, ApJ, 737, 103
Schlegel D. J., Finkbeiner D. P., David M., 1998, ApJ, 500
Shetrone M., Venn K. A., Tolstoy E., Primas F., Hill V., Kaufer A., 2003, AJ, 125, 684
Simmerer J., Sneden C., Cowan J. J., Collier J., Woolf V. M., Lawler J. E., 2004, ApJ, 617, 1091
Simon J. D., Frebel A., McWilliam A., Kirby E. N., Thompson I. B., 2010, ApJ, 716, 446
Simon J. D. et al., 2011, ApJ, 733, 46
Simon J. D., Jacobson H. R., Frebel A., Thompson I. B., Adams J. J., Shectman S. A., 2015a, ApJ, 802, 93
Simon J. D. et al., 2015b, ApJ, 808, 95
Skúldóttir Á., Andrievsky S. M., Tolstoy E., Hill V., Salvadori S., Korotin S. A., Pettini M., 2015, A&A, 580, 129
Sneden C., 1973, PhD Thesis, Univ. Texas at Austin
Sobeck J. S. et al., 2011, AJ, 141, 175
Starkenburg E. et al., 2013, A&A, 549, 88
Starkenburg E., Shetrone M. D., McConnachie A. W., Venn K. A., 2014, MNRAS, 441, 1217
Tafelmeyer M. et al., 2010, A&A, 524, A58
Tollerud E. J., Bullock J. S., Strigari L. E., Willman B., 2008, ApJ, 688, 277
Tolstoy E., Hill V., Tosi M., 2009, ARA&A, 47, 371
Tonry J. L. et al., 2012, ApJ, 750, 99
Venn K. A., Irwin M., Shetrone M. D., Tout C. A., Hill V., Tolstoy E., 2004, AJ, 128, 1177
Venn K. A. et al., 2012, ApJ, 751, 102
Ventura P., D'Antona F., Di Criscienzo M., Carini R., D'Ercole A., Vesperini E., 2012, ApJ, 761, 30
Vincenzo F., Matteucci F., Vattakunnel S., Lanfranchi G. A., 2014, MNRAS, 441, 2815
Willman B. et al., 2005, ApJ, 626, 85
Willman B., Geha M., Strader J., Strigari L. E., Simon J. D., Kirby E., Ho N., Warres A., 2011, AJ, 142, 128
Wise J. H., Turk M. J., Norman M. L., Abel T., 2012, ApJ, 745, 50
Woosley S. E., Weaver T. A., 1995, ApJS, 101, 181
Yong D. et al., 2013, ApJ, 762, 26

This paper has been typeset from a TEX/LATEX file prepared by the author.